Acta Mech
DOI 10.1007/s00707-012-0633-0

Victor Giurgiutiu · Matthieu Gresil · Bin Lin · Adrian Cuc · Yanfeng Shen · Catalin Roman

Predictive modeling of piezoelectric wafer active sensors interaction with high-frequency structural waves and vibration

Received: 12 June 2011

Abstract The modeling of the interaction between piezoelectric wafer active sensors (PWAS) and structural waves and vibration is addressed. Three main issues are discussed: (a) modeling of pitch-catch ultrasonic waves between a PWAS transmitter and a PWAS receiver by comparison between exact Lamb wave solutions and various finite element method (FEM) results; (b) analytical modeling of the power and energy transduction between PWAS and ultrasonic guided waves highlighting the tuning opportunities between PWAS and the waves; (c) the use of the transfer matrix method to model the electromechanical (E/M) impedance method for direct reading of high-frequency local structural vibration and comparison with FEM results. The paper ends with a summary and conclusions followed by recommendations for further work.

1 Introduction

An accurate predictive modeling is essential for designing effective structural health monitoring (SHM) and adaptive smart structures (ASS) applications. The main premise of our work is that commercial finite element method (FEM) codes (though easy to use and popular) have certain limitations that need to be understood. On the one hand, the FEM computational time could be extensive in the case of high-frequency (HF) structural waves and vibration because meshes finer than 1/20 of the smallest wavelength and time steps less than 1/20 of the smallest time period need to be used. Hence, wide parameter studies are impractical with FEM simulation. Analytical methods, on the other hand, are fast and efficient; they may be preferable for wide parameter studies provided the capture adequately the interaction between piezoelectric wafer active sensors (PWAS) and the HF structural waves and vibration. The purpose of this paper is to critically evaluate such analytical and numerical methods in comparison with experimental measurements.

2 Modeling of ultrasonic guided waves pitch-catch between PWAS transmitter and PWAS receiver

Figure 1 shows a pitch-catch configuration in which ultrasonic Lamb waves are sent by a transmitter PWAS and captured by a receiver PWAS, both of length $l = 2a$. Such a pitch-catch process has been simulated analytically, modeled with the finite element method (FEM), and measured experimentally.

2.1 Analytical modeling of the PWAS pitch-catch process

The analytical modeling of the pitch-catch process between two PWAS transducers separated by a distance x was carried out in frequency domain in four steps: (i) Fourier transform the time-domain excitation

Dedicated to Professor Hans Irschik on the occasion of his 60th birthday.

V. Giurgiutiu (✉) · M. Gresil · B. Lin · A. Cuc · Y. Shen · C. Roman
University of South Carolina (USC), Columbia, SC, USA
E-mail: victorg@sc.edu

Published online: 18 March 2012

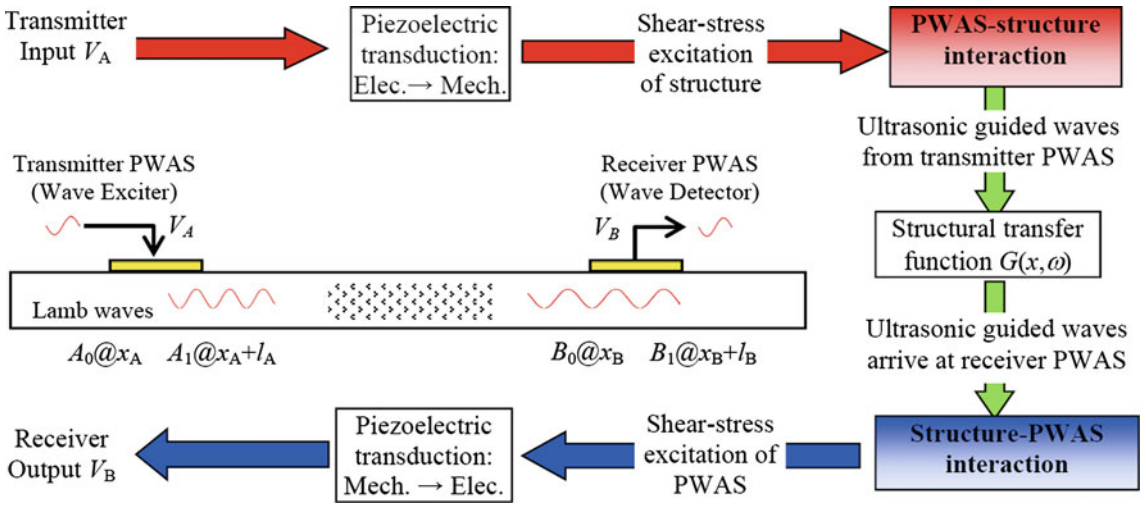

Fig. 1 A pitch-catch configuration between a transmitter PWAS and a receiver PWAS

signal $V_e(t)$ into the frequency-domain spectrum, $\tilde{V}_e(\omega)$; (ii) calculate the frequency-domain structural transfer function at the receiver location, $G(x, \omega)$; (iii) multiply the structural transfer function by frequency-domain excitation signal to obtain the frequency-domain signal at the receiver, that is, $\tilde{V}_r(x, \omega) = G(x, \omega) \cdot \tilde{V}_e(\omega)$; (iv) perform inverse Fourier transform to obtain $V_r(x, t) = \text{IFFT}\{\tilde{V}_r(x, \omega)\} = \text{IFFT}\{G(x, \omega) \cdot \tilde{V}_e(\omega)\}$, that is, the time-domain receiver signal. The structure transfer function $G(x, \omega)$ is given by Eq. (99) of Ref. [1], page 327, which gives the in-plane strain at the plate surface as

$$\varepsilon_x(x, t) = -i\frac{a\tau_0}{\mu}\left\{\sum_{\xi^S}(\sin\xi^S a)\frac{N_S(\xi^S)}{D'_S(\xi^S)}\mathrm{e}^{-i(\xi^S x-\omega t)} + \sum_{\xi^A}(\sin\xi^A a)\frac{N_A(\xi^A)}{D'_A(\xi^A)}\mathrm{e}^{-i(\xi^A x-\omega t)}\right\}, \tag{1}$$

where ξ is the frequency-dependent wave number of each Lamb wave mode and the superscripts S and A refer to symmetric and antisymmetric Lamb wave modes. The notations of Ref. [1] page 321–329 are adopted. If only the two fundamental modes, S0 and A0, are present, then $G(\omega)$ can be written as

$$\begin{aligned} G(x, \omega) &= S(\omega)\,\mathrm{e}^{-i\xi^S x} + A(\omega)\,\mathrm{e}^{-i\xi^A x}, \\ S(\omega) &= \kappa_{\text{PWAS}}\sin\xi^S a\frac{N_S(\xi^S)}{D'_S(\xi^S)}, \quad A(\omega) = \kappa_{\text{PWAS}}\sin\xi^A a\frac{N_A(\xi^A)}{D'_A(\xi^A)}, \end{aligned} \tag{2}$$

where κ_{PWAS} is the complex transduction coefficient that converts applied strain into PWAS voltage. The modal participation functions $S(\omega)$ and $A(\omega)$ determine the amplitude of the S0 and A0 wave modes excited into the structure. The terms $\sin(\xi^S a)$ and $\sin(\xi^A a)$ control the tuning between the PWAS transducer and the Lamb waves. Hence, the signal at the receiver PWAS is

$$V_r(x, \omega) = S(\omega)\,\tilde{V}_e(\omega)\mathrm{e}^{-i\xi^S x} + A(\omega)\,\tilde{V}_e(\omega)\mathrm{e}^{-i\xi^A x}. \tag{3}$$

2.2 Finite element modeling of 1-D PWAS pitch-catch process

1-D wave propagation FEM modeling is done under the z-invariant (plane-strain) assumption. Hence, only the plate cross-section needs to be meshed. For wave propagation modeling, the choice of the solving technique, mesh density, and time step influences the outcomes and level of accuracy with which the phenomenon is simulated. We used the time-domain explicit solver of the ABAQUS software and the linear quadrilateral CPE4R element. A surface-mounted transmitter PWAS was simulated with a pair of self-equilibrating forces applied at the PWAS edges. The pickup PWAS receiver placed at $x = 100$ mm was simulated by recording the in-plane strain at the PWAS location.

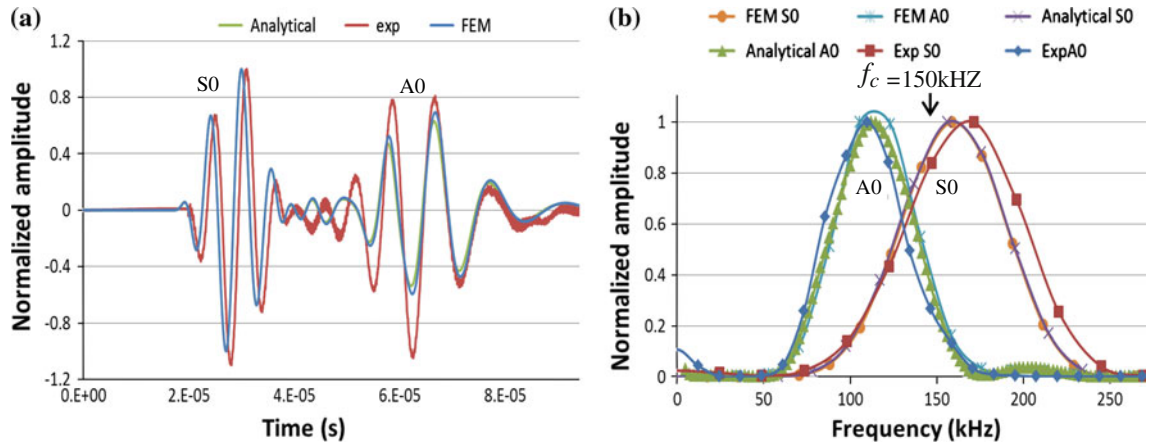

Fig. 2 Comparison of analytical, FEM, and experimental received signal for pitch-catch between two 7-mm PWAS placed 100-mm apart and excited with a 150-kHz smoothed tone burst **a** time-domain signal, **b** frequency contents of the A0 and S0 packets

In preliminary studies [2], we investigate how the group velocities of the S0 and A0 waves vary with mesh density (nodes per wavelength) $N = \lambda/L$, where λ is the wavelength and L is the size of the element. For the A0 mode, the error varies from ~9% for $N = 15$ to ~0.2% for $N = 254$. For the S0 mode, the error varies from ~2% for $N = 20$ to ~0.15% for $N = 120$. In our work, we considered a 150 kHz 3-count Hanning windowed tone burst. We choose a mesh size of 0.1 mm corresponding to $N = 76$, which mitigated a reasonable accuracy with an acceptable computation time.

2.3 PWAS pitch-catch experiments

A series of pitch-catch experiments were carried out to verify the analytical modeling and finite element simulation. A 1-mm-thick 2024-T3 aluminum plate was instrumented with a pair of 7-mm square PWAS transducers set 100 mm apart. A HP 33120A Function Generator was used to generate a 3-count Hanning windowed modulated tune burst applied to the transmitter PWAS. A TDS5034B Digital Oscilloscope was used to capture the signal at the receiver PWAS.

2.4 Discussion of pitch-catch results

The results of analytical modeling, FEM modeling, and experiments are compared in Fig. 2a; S0 and A0 mode wave packages can be observed; the wave speed of S0 mode is higher than the A0 mode, and hence, the S0 wave packet arrives earlier than the A0 wave packet. The frequency contents of these signals are shown in Fig. 2b. Comparing with the excitation frequency of $f_c = 150$ kHz, we notice that the A0 mode experienced a downward shift toward lower frequencies while the S0 mode experienced an upward shift toward higher frequencies. These shifts can be explained through the interplay between the excitation spectrum $\tilde{V}_e(\omega)$ and the PWAS tuning spectrum. Examination of Eq. (2) reveals that the S0 and A0 parts of the signal are products between the excitation spectrum and the modal participation functions $S(\omega)$ and $A(\omega)$. The resulting spectra show the observed upward and downward shifts (Fig. 3). It is interesting to note that these shifts are specific to excitation through a finite-dimensional PWAS, which has its own tuning spectrum. If the excitation was done through a point force (i.e., $a \to 0$) then such shifts are not present because the spectrum of the associated Dirac function is flat in the frequency domain.

2.5 Multi-physics FEM modeling of 2-D PWAS pitch-catch process

The use of multi-physics finite element method (MP-FEM) allows us to apply directly the excitation voltage at the transmitter PWAS (T-PWAS) and record directly the capture signal at the receiver PWAS (R-PWAS).

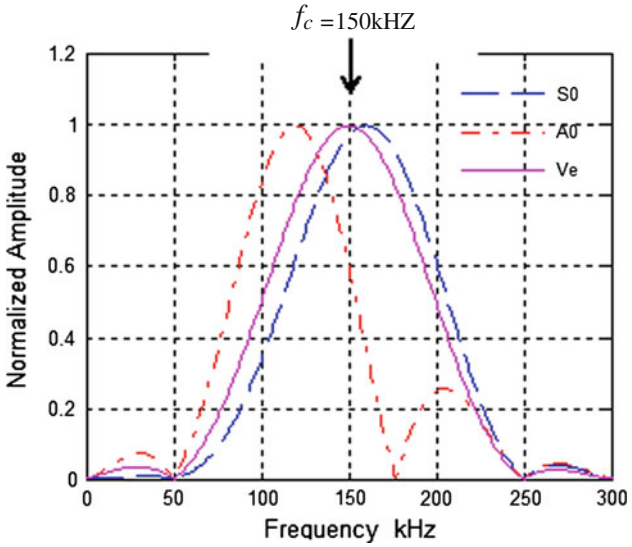

Fig. 3 Analytical S0 and A0 wave spectra compared with excitation spectrum V_e at 150 kHz

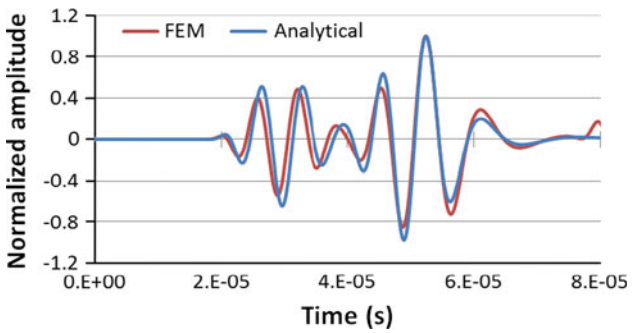

Fig. 4 Comparison between the analytical and FEM simulated signals at the PWAS receiver

We used the ABAQUS implicit code to simulate the generation of Lamb waves in a 2-mm steel plate with surface-mounted 7-mm square PWAS placed 100 mm apart [3]. The plate was discretized with C3D8R brick elements of size 0.5 mm (mesh density $N = 15$ elements per wavelength). The PWAS transducers were discretized with the C3D8E piezoelectric element. We modeled directly the electric signal recorded at the R-PWAS due to an electric excitation applied to the T-PWAS, which generated ultrasonic guided waves traveling through the plate. Figure 4 shows the comparison between the analytical signal and the MP-FEM signal for a 3-count smoothed tone burst excitation. It is apparent that both the A0 and S0 waves are well simulated by the MP-FEM technique.

3 Modeling of power and energy transduction for SHM applications

A preliminary analysis of the 1-D and 2-D power and energy transduction process for SHM applications was performed using analytical tools [4–6]. Figure 1 shows the power and energy transduction flow chart for a pitch-catch setup between a transmitter PWAS and a receiver PWAS. The following assumptions were used: (a) ideal bonding connection between PWAS and structure; (b) ideal excitation source at the transmitter PWAS and fully resistive external load at the receiver PWAS; and (c) axial and flexural wave propagation. To perform this analysis, Lin and Giurgiutiu [4,5] developed 1-D and 2-D closed form analytical expressions for the active and reactive electrical power, mechanical power in the PWAS, and ultrasonic acoustic power of the waves traveling in the structure. The simulation considered two PWAS (a transmitter and a receiver) attached on a simple aluminum structure. The electrical active power, reactive power, and power rating for harmonic voltage excitation were examined for both 1-D [4] and 2-D [5] geometries. The analysis was performed in the simplifying case of only axial and flexural waves, which are easier to handle than the full multi-mode guided-wave

analysis. However, the principles of this exploratory study can be extended without much difficulty to the full multi-mode guided-wave analysis.

3.1 Power and energy transduction

There are three parts in the power flow: transmitter PWAS power and energy, wave propagation power and energy in structure, and receiver PWAS power and energy. In pitch-catch mode (Fig. 1), the power flow converts from electrical source into piezoelectric power at the transmitter, the piezoelectric transduction converts the electrical power into the mechanical interface power at the transmitter PWAS and then into acoustic wave power traveling in the structure. The wave power arriving at the receiver PWAS is captured through the mechanical interface between the PWAS and the structure and converted back into electrical power that is recorded by the receiver electric instrumentation. The time-averaged electrical power, mechanical power at the transmitter, and wave power can be calculated from the frequency response function.

3.2 Transmitter PWAS power and energy

The electrical energy of the input voltage applied at the transmitter PWAS terminals is converted through piezoelectric transduction into mechanical energy of the PWAS transducer expansion–contraction motion. This motion is transmitted to the underlying structure through the shear stress in the adhesive layer at the PWAS-structure interface. As a result, ultrasonic guided waves are excited into the underlying structure. The mechanical power at the interface becomes the acoustic wave power and the generated axial and flexural waves propagate in the structure. Several questions need to be answered: (i) how much of the applied electrical energy is converted into the wave energy? (ii) how much of the applied electrical energy gets rejected back into the electrical source? (iii) how much energy is lost through the shear transfer at the PWAS-structure interface? and (iv) what are the optimal combinations of PWAS geometry, excitation frequency, and wave mode to inject the maximum energy as ultrasonic waves into the structure?

3.2.1 Active and reactive parts of the electrical power input

The electrical active power applied to the transmitter PWAS is actually the power that gets converted into the ultrasonic acoustic waves generated by the PWAS into the structure. This is the useful part of the power input. However, our analysis revealed that the reactive part of the electrical power input can be orders of magnitude larger than the active power because the PWAS transducer is essentially a capacitive device, and its admittance is dominated by $Y_C = i\omega C$. Hence, power sources capable of recirculating the reactive power should be used for efficient PWAS excitation; otherwise, the power rating of the excitation source must be much larger than the actual active power injected into the structure.

3.2.2 Active power conversion into ultrasonic wave power

The electrical active power converts into the ultrasonic wave power through piezoelectric transduction in the PWAS and shear lag transfer at the PWAS-structure interface. In a 1-D analysis, the PWAS transmitter generates ultrasonic waves traveling both forward and backward from it. Our analysis [4] indicated that the sum of the powers of the forward and backward waves emanating from the PWAS matches exactly the electrical active power applied to the PWAS. In a 2-D geometry, a circular PWAS generates circular-crested ultrasonic waves emanating from it. Our analysis [5] revealed that the electrical active power converts exactly into the power of these circular-crested ultrasonic waves emanating from the transmitter PWAS.

3.2.3 PWAS size tuning effects

In 1-D modeling [4], a PWAS of length $l = 2a$ generates an in-plane surface strain containing the effect of both axial and flexural waves in the form

$$\varepsilon(t) = i\varepsilon_0 \mathrm{e}^{-i\omega t} \left\{ \sin(\xi_0 a)\, \mathrm{e}^{i\xi_0(x-x_0-a)} + 3\sin(\xi_F a)\, \mathrm{e}^{i\xi_F(x-x_0-a)} \right\}. \tag{4}$$

In 2-D modeling [5], a circular PWAS of radius a generates circular-crested axial and flexural waves with an in-plane surface strain of the form

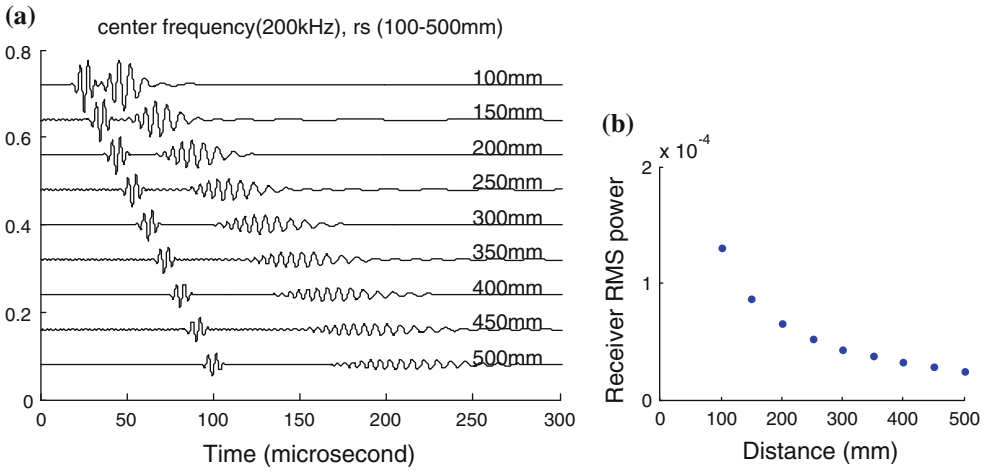

Fig. 5 Pitch-catch signal with a receiver PWAS **a** at different distance from a transmitter PWAS, **b** RMS power of a receiver at different distance

$$\varepsilon(t) = i\pi a\varepsilon_0 e^{-i\omega t}\left\{J_1(\xi_0 a)\, J_1(\xi_0 r) + 3J_1(\xi_F a)\, J_1(\xi_F r)\right\}. \tag{5}$$

Optimal wave excitation can be obtained when the PWAS length is an odd multiple of the half wavelength, whereas even multiples lead to wave rejection. Since, at a given frequency, the axial and flexural waves have different wavelengths, opportunities arise for tuning into one or the other of these waves through tuning of PWAS size and excitation frequency.

Due to the tuning effects, the wave power (and hence the electrical active power input) is not constant, but presents a peaks and valleys pattern that corresponds to the PWAS tuning in and out of the ultrasonic waves traveling into the structure. The maximum wave power injected into a 1-D structure (1-mm-thick 2,024 aluminum strip) by a 7-mm PWAS under 10-V harmonic seems to be ~80 mW at ~420 kHz.

3.3 2-D simulation of PWAS power and energy

For 2-D analysis, we considered two 7-mm-diameter, 0.2-mm-thick circular PWAS transducers placed on a 1-mm-thick 2,024 aluminum plate in a pitch-catch configuration. A 10-V 100-kHz 3-count Hanning windowed tone burst was applied to the transmitter PWAS. The voltage signals received at various distances from the source are shown in Fig. 5a. The nondispersive fast axial wave is clearly separated from the dispersive slower flexural wave. Figure 5b gives a plot of the received RMS power ($\text{RMS} = \sqrt{\int_0^\tau V^2 dt/\tau}$). It is apparent that the received RMS power varies with $1/r$, as expected.

3.3.1 Parametric study of PWAS power and energy

A parametric study of the effect of transmitter size and impedance, receiver size and impedance, and external electrical load gives the PWAS design guideline for PWAS sensing and power harvesting applications. Figure 6 presents the results for various PWAS sizes and frequencies. 2-D of circular-crested axial and flexural waves emanating from a circular PWAS were considered. The power-rating plot of Fig. 6a shows a monotonic increase with frequency and PWAS size: to drive a 15-mm PWAS at 1,000 kHz with a 10 V constant input, one needs a power source providing 10 W of reactive power. The actual wave power that the PWAS would inject into the structure varies up and down with frequency and PWAS size as shown in Fig. 6b; it is apparent that tuning combinations of PWAS size and excitation frequency can produce excitation 'sweet spots' as well as wave rejections. As a general rule, one should remember that, at a given frequency, a larger PWAS would require a larger reactive power but will not necessarily produce more wave power into the structure. The maximum wave power output in this 2-D simulation was ~20 mW.

The power contained in the axial waves and flexural waves is given separately in Fig. 6c and d. In some PWAS SHM applications, a single mode is often desired to reduce signal complexity and simplify signal interpretation and damage detection. Figure 6c shows the frequency-size combinations at which the axial waves

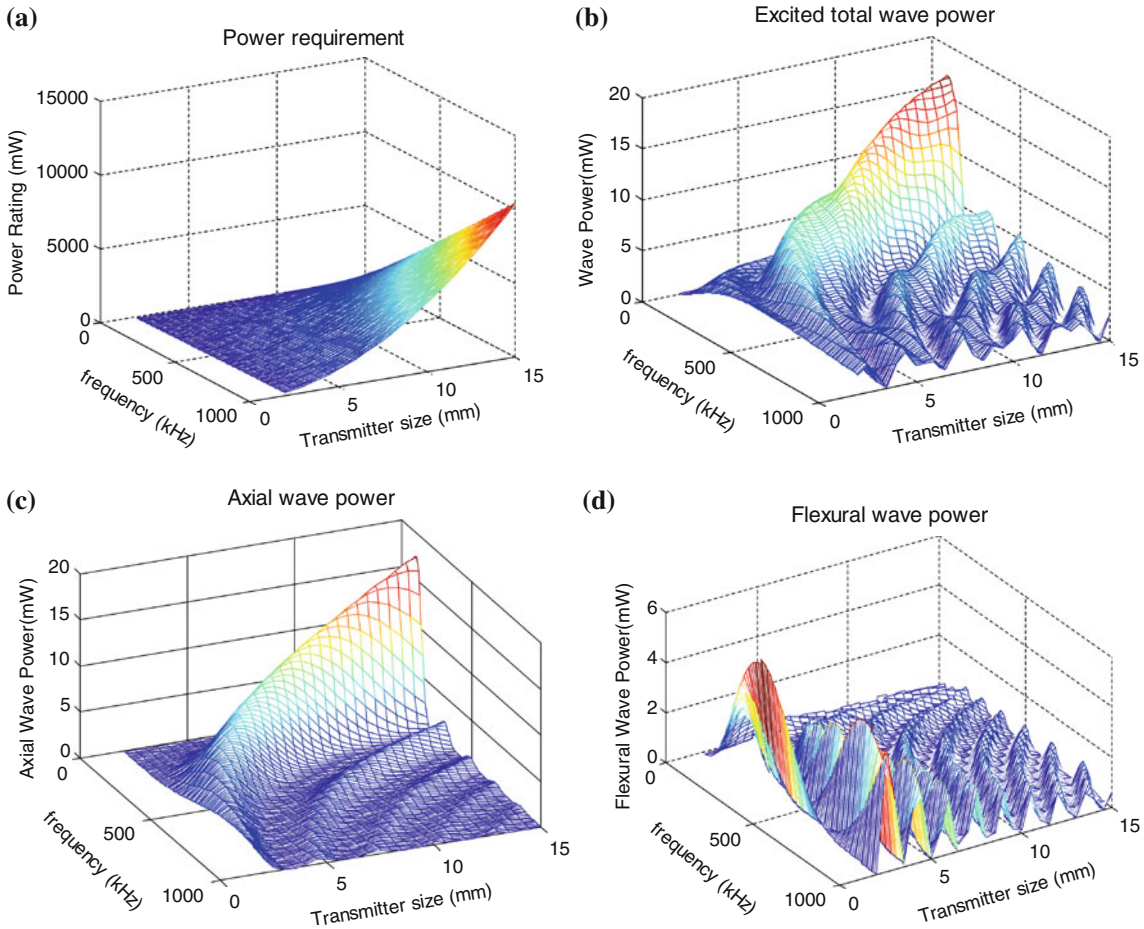

Fig. 6 PWAS transmitter under constant voltage excitation **a** power rating, **b** wave power, **c** axial wave power, **d** flexural power

are maximized, whereas Fig. 6d indicates the combinations that would maximize the flexural waves. These figures give useful guidelines for the choosing PWAS size and frequency values that are optimum for selecting a certain excitation wave mode. This study gives guidelines for selection of transmitter size and excitation frequency to obtain maximum wave power into the SHM structure.

3.4 Receiver power and energy

Similar tuning effects were observed at the receiver PWAS. Receiver PWAS has a similar size as transmitter PWAS. When structural waves reach the receiver PWAS, the wave energy is converted into electrical energy displayed as a voltage signal. For sensing application, a high value of the output voltage can be obtained by setting to 'high impedance' the electrical load of the external measuring device (e.g., a digitizing oscilloscope) connected to the PWAS. Thus, the current absorbed by the PWAS is kept very much. Although the measure voltage is quite large, the actual power energy is picked up by PWAS is very small. For power harvesting application, the receiver PWAS must be matched electrically with the external electrical load impedance in order to maximize the output power.

4 Transfer matrix method modeling of PWAS electromechanical (E/M) impedance response

The transfer matrix method (TMM) is an analytical method for structural analysis, which is an alternative to modal expansion. The TMM principle is to break up the structure into smaller components across which one calculates the transfer of a state vector (displacements and forces). Pestel and Leckie [7] introduced the TMM

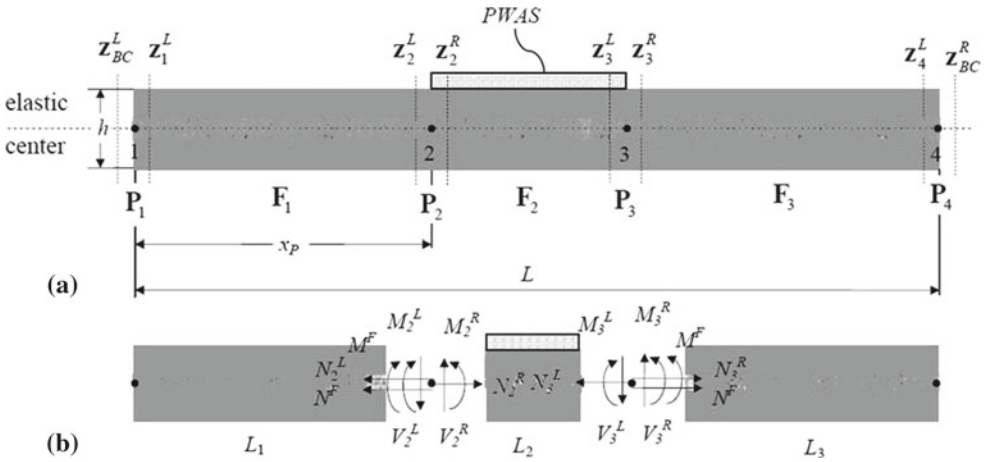

Fig. 7 Multi-layer beam under PWAS excitation **a** schematic of beam elements, **b** free-body diagram

concept in the 1960s. Giurgiutiu and Stafford [8] used TMM to calculate the vibration of helicopter blades modeled as rotating Timoshenko beams. Bois et al. [9,10] used TMM to calculate the electromechanical (E/M) impedance of a PWAS mounted on a composite beam with internal delaminations. Cuc [11] applied TMM to bonded metallic beams. TMM uses general analytical solutions for axial and flexural vibration of a uniform beam to expresses the state vector $\mathbf{z}(x)$ at a location x as the product between a matrix of solution functions, $\mathbf{B}(x, \omega)$, and a column of coefficients, $\mathbf{a}$, that is,

$$\begin{aligned} \mathbf{z}(x) &= \mathbf{B}(x, \omega)\,\mathbf{a}, \\ \mathbf{z} &= \left[\, u \;\; w \;\; \phi \;\; N \;\; M \;\; V \,\right]^T, \quad \mathbf{a} = \left[\, A_1 \;\; A_2 \;\; A_3 \;\; A_4 \;\; A_5 \;\; A_6 \,\right]^T. \end{aligned} \tag{6}$$

For example, the displacements $u(x)$ and $w(x)$ can be expressed as

$$u(x) = \sum_{i=1,2} A_i g_j(x, \omega), \quad w(x) = \sum_{j=1,2,3,4} A_{j+2} f_j(x, \omega), \tag{7}$$

$$\begin{aligned} g_1(x, \omega) &= \sin\left[\gamma_a(\omega)\, x\right]; \quad g_2(x, \omega) = \cos\left[\gamma_a(\omega)\, x\right], \\ f_1(x, \omega) &= \frac{1}{2}\left\{\cosh\left[\gamma_f(\omega)\, x\right] + \cos\left[\gamma_f(\omega)\, x\right]\right\}, \\ f_2(x, \omega) &= \frac{1}{2\gamma_f(\omega)}\left\{\sinh\left[\gamma_f(\omega)\, x\right] + \sin\left[\gamma_f(\omega)\, x\right]\right\}, \\ f_3(x, \omega) &= \frac{1}{2\gamma_f^2(\omega)}\left\{\cosh\left[\gamma_f(\omega)\, x\right] - \cos\left[\gamma_f(\omega)\, x\right]\right\}, \\ f_4(x, \omega) &= \frac{1}{2\gamma_f^2(\omega)}\left\{\sinh\left[\gamma_f(\omega)\, x\right] - \sin\left[\gamma_f(\omega)\, x\right]\right\}, \end{aligned} \tag{8}$$

where $\gamma_a(\omega) = \omega\sqrt{m/EA}$, $\gamma_f(\omega) = (m/EI)^{1/4}\sqrt{\omega}$ are axial and flexural wavenumbers, respectively. Consider now a larger beam divided in N segments. For each segment, the state vector at one end can be expressed in terms of the state vector at the other end and a field transfer matrix $\mathbf{F}_i$, that is,

$$\mathbf{z}_i = \mathbf{F}_i \mathbf{z}_{i-1}, \quad \mathbf{F}_i = \mathbf{B}(l_i)\,\mathbf{B}^{-1}(0), \quad i = 0, 1, \ldots N. \tag{9}$$

At the interface between two segments, one can also apply point transfer matrices $\mathbf{P}_i$ such that $\mathbf{z}_i^R = \mathbf{P}_i \mathbf{z}_i^L$, where the superscript L or R denotes the left or the right sides. By repeated application of this process one can express the state vector at the end of a large beam $\mathbf{z}_N$ in terms of the state vector $\mathbf{z}_0$ at the beginning of the beam and an overall transfer matrix $\mathbf{U}$, that is,

$$\mathbf{z}_N = \mathbf{U}\mathbf{z}_0, \;\; \text{where } \mathbf{U} = \mathbf{F}_N \cdot \mathbf{P}_{N-1} \cdot \mathbf{F}_{N-1} \;\cdots\; \mathbf{F}_2 \cdot \mathbf{P}_1 \cdot \mathbf{F}_1. \tag{10}$$

The state vectors at the beginning and the end of the beam, $\mathbf{z}_0$ and $\mathbf{z}_N$, satisfy the boundary conditions which can be prescribed displacements or applied forces.

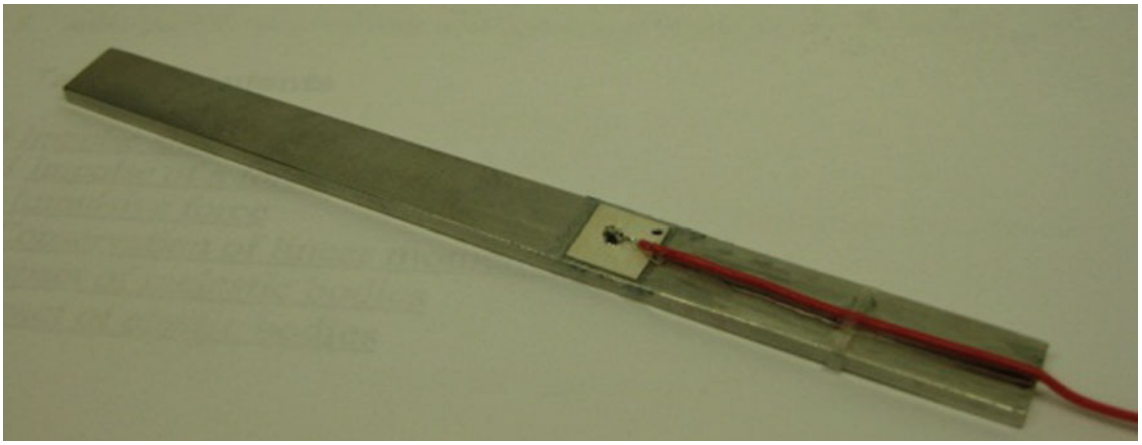

Fig. 8 Beam specimen with bonded PWAS

4.1 TMM simulation of E/M impedance method

The TMM approach was used to predict the E/M impedance response of a PWAS attached to a free–free beam. As shown in Fig. 7, the beam was divided into three segments, of which the middle segment represents the zone covered by the PWAS. The equivalent material properties along the elastic axis, the field and point transfer matrices at each segment and the overall transfer matrix, **U**, were calculated. Partitioning of **z** into displacement and force parts, $\mathbf{z} = \left\{ \mathbf{d}\ \mathbf{p} \right\}^t$, followed by partition of **U** and rearrangement yields the linear system

$$\begin{bmatrix} -\mathbf{U}_{dd} & \mathbf{I} \\ -\mathbf{U}_{pd} & \mathbf{0} \end{bmatrix} \cdot \begin{bmatrix} \mathbf{d}_{BC}^{L} \\ \mathbf{d}_{BC}^{R} \end{bmatrix} = \begin{bmatrix} \mathbf{U}_{dp} & \mathbf{0} \\ \mathbf{U}_{pp} & \mathbf{I} \end{bmatrix} \cdot \begin{bmatrix} \mathbf{p}_1^F \\ \mathbf{p}_2^F \end{bmatrix} \text{ or, in matrix form, } \quad \mathbf{M} \cdot \mathbf{X} = \mathbf{N}. \tag{11}$$

Upon solution, one finds the end displacements and hence the state vectors at the beam ends. Starting from the left-hand side end, one calculates the coefficients vectors $\mathbf{a}_i$ and hence the displacement distribution, that is,

$$\mathbf{z}_{BC}^{L} = \mathbf{B}\,(0,\omega) \cdot \mathbf{a} \quad \Rightarrow \quad \mathbf{a}_1 = \mathbf{B}^{-1}\,(0,\omega) \cdot \mathbf{z}_{BC}^{L} = \left\{ A_1^1 \ \ldots \ A_6^1 \right\}^t, \text{ etc.} \tag{12}$$

To calculate the E/M impedance, we need to calculate the dynamic stiffness $k_{str}(\omega)$ presented by the beam to the PWAS. Following Ref. [1], page 371, we calculate the displacement differential between the ends of the surface-mounted PWAS, that is,

$$\Delta u = u\,(x_2) - u\,(x_1) - \frac{h}{2}\left[w'(x_2) - w'(x_1)\right] \quad \text{or} \quad \Delta u = \left(u_3^L - u_2^R\right) - \frac{h}{2}\left(\varphi_3^L - \varphi_2^R\right). \tag{13}$$

The dynamic stiffness $k_{str}(\omega)$ is the inverse of the frequency response function and has the expression

$$k_{str} = 1/FRF(\omega) = (\Delta u/F)^{-1} = F/\left\{\left(u_3^L - u_2^R\right) - \frac{h}{2}\left(\varphi_3^L - \varphi_2^R\right)\right\}. \tag{14}$$

According to Giurgiutiu [1] knowing the material properties and the dimensions of the PWAS the electro-mechanical impedance can be expressed as

$$Z = \frac{1}{Y} = \frac{1}{i\omega C}\left[1 - \kappa_{31}^2\left(1 - \frac{1}{\varphi\cot\varphi + r}\right)\right]^{-1}, \quad \varphi(\omega) = \frac{1}{2}\omega\rho_p s_{11}^E l_p, \quad r(\omega) = \frac{k_{str}(\omega)}{k_{\text{PWAS}}}. \tag{15}$$

4.2 Comparison of analytical, TMM, FEM, and experimental results

A small $10 \times 8 \times 2.035\,\text{mm}^3$ beam specimen was machined out of 304 stainless steel. A $7 \times 7 \times 0.2\,\text{mm}^3$ PWAS was bonded to the beam at $x = 60\,\text{mm}$ from the left side of the beam (Fig. 8). The E/M impedance was recorded with an HP4194A Impedance Analyzer in the range 10–100 KHz and used for comparison with analytical and FEM predictions.

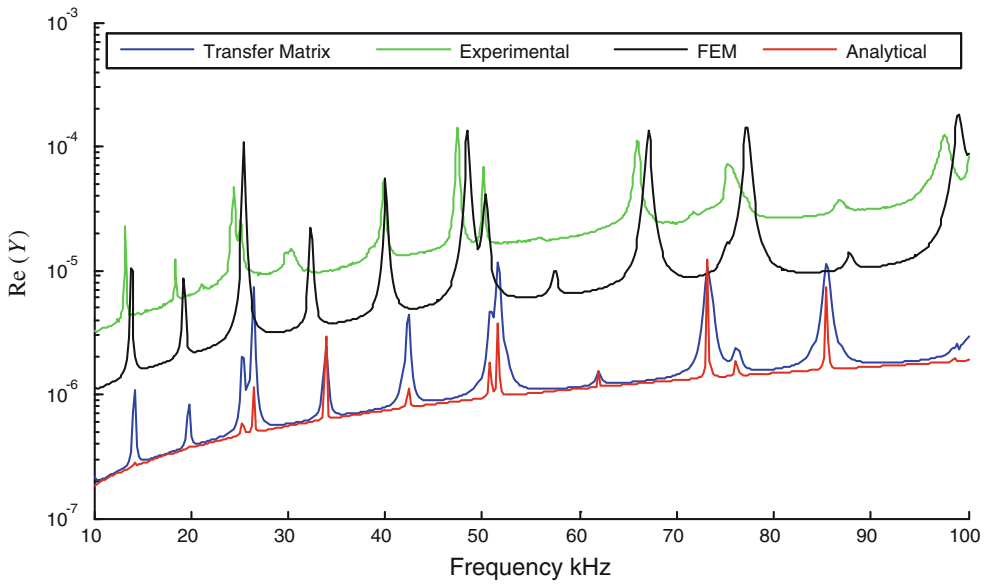

Fig. 9 Experimental admittance compared with predictions by analytical modal analysis, analytical TMM, and 3D MP-FEM

Three different ANSYS FEM modules were used. The Workbench (WB) module was used to compute the natural frequencies of the beam. The 2-D multiphysics module (2D MP-FEM) was used to calculate directly the E/M impedance under the plane-strain assumption; the beam was modeled with the conventional 8-node PLANE82 (two dof/node), whereas the PWAS was modeled with the multiphysics 8-node PLANE223 with up to four dof/node. The 3D MP-FEM analysis allowed realistic 3D modeling of the actual specimen and PWAS; the 20-node SOLID95 element was used for the beam and the 20-node multiphysics SOLID226 for the PWAS. A 1-mm mesh size was used. In both 2D and 3D MP-FEM analyses, the impedance was calculated directly as the complex ratio between the voltage applied to the PWAS and the corresponding charge rate. Figure 9 plots the experimental admittance Re(Y) compared with predictions by analytical modal analysis, analytical TMM, and 3D MP-FEM. It is apparent that the modal analysis and TMM approaches give very similar results since both are based on analytical assumptions; they predicted the resonance peaks quite well but were orders of magnitude off in terms of the vertical position of the admittance dereverberated baseline. The 3D MP-FEM gave much better prediction of the vertical position of the dereverberated baseline, but missed the splitting of the peak at ∼26 kHz.

5 Conclusion

This paper has discussed the modeling of the interaction between PWAS and high-frequency structural waves and vibration. Three main issues are considered: (a) modeling of pitch-catch ultrasonic waves between a PWAS transmitter and a PWAS receiver by comparison between exact Lamb wave solutions and various FEM results; (b) analytical modeling of the power and energy transduction between PWAS and ultrasonic guided waves highlighting the tuning opportunities between PWAS and the waves; (c) the use of the transfer matrix method (TMM) to model the electromechanical (E/M) impedance method for direct reading of HF local structural vibration and comparison with FEM results.

It was found that both the analytical and FEM predictions of HF wave propagation agreed well with the experimental results. An important phenomenon was observed both experimentally and in simulations: the central frequency $f_c = 150$ kHz of an excitation tone burst was not exactly recovered in the A0 and S0 ultrasonic wave packets; the A0 central frequency was shifted downward, whereas the S0 frequency was shifted slightly upward. Moreover, at other excitation frequencies (e.g., $f_c = 600$ kHz), the shift direction was reversed (S0 downward, A0 upward). Nonetheless, these shifts were analytically explained as the interplay between excitation spectrum and PWAS tuning spectrum.

The multi-physics finite element method (MP-FEM) was found effective in predicting directly the electrical signal at a receiver PWAS in response to a given excitation at a transmitter PWAS, provided the mesh size and

time step were sufficiently small (e.g., 1/20 of the smallest wavelength and time period). This greatly simplifies the modeling effort because MP-FEM accounts implicitly for all the electromechanical (E/M) transduction steps. In the case of E/M impedance modeling, the MP-FEM approach was found to be closer to the measurements than the analytical methods (modal expansion and TMM). Nonetheless, both analytical and MP-FEM methods were quite accurate in the prediction of the measured structural resonances.

The prediction of power and energy (P&E) requirements for PWAS based smart systems is essential for good system design. The analytical P&E predictions presented in this paper indicated two important aspects. First, the reactive part of the electrical power can be orders of magnitudes larger than the active part because PWAS is an essentially capacitive device. However, only the active part of the electrical power gets transducted into the structural waves. Hence, electrical power sources capable of properly handling (i.e., recirculating) the reactive power should be used. Second, the ultrasonic wave power injected into the structure varies considerably with both PWAS size and excitation frequency. The parameter studies reported in this paper revealed peaks and valleys in the wave power spectrum that could be exploited in the system design in order to achieve maximum benefits with minimum P&E expenditure.

Future work should focus on extending the current work toward predictive modeling of more realistic structures with complicated actual constructive details. The complexity posed by modern high-performance materials (composites, hybrids, etc.) should be addressed. The P&E analysis should be extended beyond the simple axial/flexural waves into HF multi-modal ultrasonic guided waves. Experimental confirmation of the P&E predictions should also be sought.

Acknowledgments Support of National Science Foundation #CMS-0925466, Shih-Chi Liu, Program Director; National Institute of Standards and Technology, #70NANB9H9007; and Office of Naval Research # N00014-11-1-0271, Dr. Ignacio Perez, Program Monitor, are thankfully acknowledged.

References

1. Giurgiutiu, V.: Structural Health Monitoring with Piezoelectric Wafer Active Sensors. Academic Press, Massachusetts (2008)
2. Gresil, M., Shen, Y., Giurgiutiu, V.: Predictive Modeling of Ultrasonics SHM with PWAS Transducers. IWSHM 2011, Stanford (in press)
3. Gresil, M., Yu, L. Giurgiutiu, V.: Fatigue crack detection in thick steel structures with piezoelectric wafer active sensors. In: Proceedings of SPIE, vol. 7983, p 79832Y (2011)
4. Lin, B., Giurgiutiu, V.: Modeling of power and energy transduction analysis of piezoelectric wafer active sensors for structural health monitoring. In: Proceedingas of SPIE, vol. 7647 (2010)
5. Lin, B., Giurgiutiu, V.: Simplified 2D modeling of power and energy transduction of piezoelectric wafer active sensors for structural health monitoring. In: Proceedings of SPIE, vol. 7981 (2011)
6. Lin, B., Giurgiutiu, V.: Power and energy transduction analysis of piezoelectric wafer active sensors for structural health monitoring. Struct. Health Monit. Int. J. **11**, 109–121
7. Pestel, E., Leckie, F.A.: Matrix Methods in Elasto-mechanics. McGraw-Hill, New York (1963)
8. Giurgiutiu, V., Stafford, R.O.: Semi–Analytic Methods for Frequencies and Mode-Shapes of Rotor Blades, Vertica, vol. 1, pp. 291–306. Pergamon Press, England (1977)
9. Bois, C., Hochard, C.: Monitoring of laminated composites delamination based on electro-mechanical impedance measurement. J. Intell. Mater. Syst. Struct. **15**, 59–67 (2004)
10. Bois, C., Herzog, P., Hochard, C.: Monitoring a delamination in a laminated composite beam using in-situ measurements and parametric identification. J Sound Vib. **299**, 786–805 (2007)
11. Cuc, A.: Structural Health Monitoring of Adhesively Bonded Joints with Piezoelectric Wafer Active Sensors. PhD Dissertation, University of South Carolina, August (2010)